Radar-based measurements of the solids flow in a circulating fluidized bed

Fuel 345 (2023) 128232

Contents lists available at ScienceDirect

Fuel

journal homepage: www.elsevier.com/locate/fuel

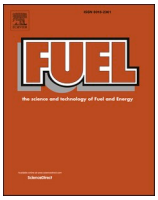

Radar-based measurements of the solids flow in a circulating fluidized bed

Diana Carolina Guío-Pérez [a,*], Marlene Bonmann [b], Tomas Bryllert [b], Martin Seemann [a], Jan Stake [b], Filip Johnsson [a], David Pallarès [a]

[a] Department of Space, Earth and Environment, Division of Energy Technology Chalmers University of Technology, SE-412 96 Gothenburg, Sweden
[b] Department of Microtechnology and Nanoscience, Terahertz and Millimetre Wave Laboratory, Chalmers University of Technology, SE-412 96 Gothenburg, Sweden

ARTICLE INFO

Keywords:
Submillimeter wave radar
Doppler
Solids flow
Solids concentration
Solids velocity
Non-intrusive technique
Circulating fluidized bed

ABSTRACT

The aim of this work is to demonstrate the value of radar technology for studying experimentally the solids flows in gas-solids fluidized beds. The work presents original results regarding the solids concentration and velocity acquired in a non-intrusive manner from a cold flow model. The tailored radar setup operates at submillimeter wave frequencies (0.34 THz) and can measure the location of solids with a spatial resolution of 1/8 mm^{-1} in the direction of the radar beam, and of 40–60 mm across the radar beam. The solids velocity in the direction of the beam propagation is determined through measurement of the Doppler shift caused by the reflection of the transmitted radar signal by solids moving in relation to the antenna. The measurements were performed in both the horizontal and vertical directions in the riser of a circulating fluidized bed (cross-sectional area of 0.45 m^2 and height of 3.1 m) operated with glass beads (mean particle size of 106 μm, and particle density of 2,486 kg/m^3) and using air at ambient temperature as the fluidization agent, with superficial velocities in the range of 0.3–1.3 m/s. The measurements are used to assess the validity of the technique and are not intended to characterize the unit fluid dynamically. The solids concentrations derived from the radar measurements follow the qualitative trends derived from pressure-drop measurements, resembling the expected changes that occur in the concentration profiles as the fluidization velocity increases. Concentrations in the range from 10^{-6} m^3/m^3 to 10^{-1} m^3/m^3 are measurable. In quantitative terms, for low concentrations of solids ($<5{\cdot}10^{-3}$ m^3/m^3, approximately) the radar measurements exhibited the ability to provide more consistent measurements of the solids concentration than those obtained from pressure transducers, for which the small pressure differences lead to unstable and even negative values for solids concentrations. The two measurement methods were in quantitative agreement for solids volume fractions higher than the threshold. Concentrations $\geq 1{\cdot}10^{-1}$ m^3/m^3, though measurable, strongly attenuate the radar signal, thereby reducing the beam penetration to a depth of centimeters. For each position along the radar beam, the distribution of solids velocity measured from the Doppler effect was found to be within the expected ranges and allowed observations of solids back-mixing. The radar technique applied in this work is a promising technique for detailed characterization of the solids flow in fluidized beds, offering high spatial and temporal resolutions, allowing the determination of both solids velocity and concentration, and having a reasonably high penetration depth.

1. Introduction

Despite the fact that the fluidized bed technology has been applied commercially for many decades, there is still incomplete understanding of the gas-solids flow in fluidized beds, especially concerning the details of the gas-solids flow. The high-level complexity of the gas-solids flow makes it very difficult to predict fully the flow using available theories, since theoretical models rely on detailed experimental data for validation. In this context, it is of special interest to develop non-intrusive techniques that can provide high-resolution spatial and temporal measurements of the solids flow.

Typically, the solids flow in a fluidized bed reactor is characterized using pressure measurements, which, although non-intrusive, only approximate the solids concentration over a region of uncertain extension [2]. Vertical pressure drop measurements in the riser provide vertical profiles of the average concentrations of the solids in the vicinity of the pressure taps [1] with a spatial resolution that corresponds to the distance between the pressure taps and with a level of accuracy that is dependent upon the resolution and sensitivity of the pressure

* Corresponding author.
E-mail address: carolina.guioperez@chalmers.se (D.C. Guío-Pérez).

https://doi.org/10.1016/j.fuel.2023.128232
Received 30 December 2022; Received in revised form 15 March 2023; Accepted 24 March 2023
Available online 2 April 2023

Nomenclature

BW Hz	Bandwidth
c_0 m/s	Speed of light
c_v m^3/m^3	Solids volume concentration
d_{radar} m	Diameter of the radar beam
f_cHz	Center frequency
f_{IF} Hz	Frequency difference
f_s Hz	Sampling frequency
f_{mix} Hz	Digital mixing frequency
f_{PSD}-	Particle size distribution probability function
G-	Antenna gain
K Wm^2	Radar calibration parameter
n_p-	Number of pulses
n_s-	Number of samples per pulse
n_{solids} #part./m^3	Solids number concentration
P_r W	Reflected signal power
P_t W	Peak transmit power
PRI	Pulse Repetition Interval
PRF	Pulse Repetition Frequency
Q_b-	Mie back-scattering efficiency
Q_e-	Mie extinction efficiency
r m	Radius of a single particle
r_{radar} m	Radius of the radar beam
R m	Radar range
R_m m	Range of axis after processing
R_R s	Round-trip delay time
v_d m/s	Velocity of the particles
v_m m/s	Velocity axis span
V_{radar} m^3	Radar sample volume
ΔR m	Range resolution
$\Delta f/\Delta t$ $s^{-}2$	Chirp rate of the frequency ramp
Δh m	Height difference
ΔP m	Pressure difference
ε_g-	Bed voidage
ρ_s kg/m^3	Solids density
ρ_g kg/m^3	Gas density
σ_b m^2	Single-target back-scattering cross-section
$\sigma_{b,tot}$ m^2	Total back-scattering cross-section
σ_e m^2	Effective extinction cross-section
θ rad	Radar angular beam width

transducers (the distance between the pressure taps is typically chosen to be a few centimeters in research units and up to several meters in commercial units). To obtain information on the spatially resolved cross-sectional distribution of the solids, other measurement techniques must be applied that require the insertion of probes over the cross-section of the reactor, which inevitably leads to disturbance of the flow [3,4]. Non-intrusive tomography techniques, such as those based on x-rays, γ-rays and electrical capacitance, have been used experimentally to conduct mapping of the solids concentration field in narrow, bench-scale units with a spatial resolution in the order of a few centimeters [5] and references therein]. While such dynamic tomographic measurements have provided valuable knowledge regarding the gas bubble flow (including bubble size and velocity), they do not assess the velocity field of the solids phase. In pharmaceutical applications, ERT (electrical resistance tomography) and ECT (electrical capacitance tomography) have been used in the characterization of the solids flow dynamics in units of up to 1 m in diameter [6]. Implementation of ECT in industrial scale combustion CFB units is envisioned, but depends on: (i) the successful development of an adequate sensor design that compensates the change in capacitance due to temperature and is able to reach high enough sensitivity in the core of the unit, (ii) the upgrading of image reconstruction algorithms for the increased number of sensors and (iii) the achievement of a reliable calibration [6,7]. Direct tracking methods, such as Particle Image Velocimetry (PIV) [8], which are used for diagnostic analyses of the particulate phase, allow for a high spatial resolution (around 1 mm) but have a limited penetration depth due to the requirement for a free line-of-sight. It may be possible to overcome these above shortcomings by applying radar technology-based measurements.

Radar technology has undergone strong development over the last few years, as an alternative to using infrared or visible light for imaging applications [9]. Imaging systems that use radar are already achieving time resolutions similar to whose of video recordings (>6 fps) [10]. In addition, the use of terahertz radiation provides the technology with the capability to penetrate many non-conducting materials [11]. The recently developed radar technology at submillimeter wave frequencies [12], inspired by weather radars that monitor gas–solid and gas–liquid dynamics in the atmosphere, has potential as an efficient way to execute non-intrusive diagnostic analyses of solids flow in fluidized beds (or other solids handling equipment). This is because it offers the possibility to measure in a non-intrusive fashion the velocities and concentrations of small (micrometer scale) solid particles with high spatial and temporal resolutions and with good penetration levels. The submillimeter wave frequency (lower than optical frequencies, which are in the range of 400–700 THz) enhances penetration into the solids suspension, which at the same time affording a frequency that is high enough (compared to weather or automotive radars) to ensure sensitivity for the detection of small particles [12]. The Frequency Modulated Continuous Wave (FMCW) feature enables the use of the same antenna for transmitting and receiving the signal, while the range-Doppler enables the determination of the velocity in the axial direction, i.e., along the direction of propagation of the radar beam. The measurement of solids concentration and solids velocity using the submillimeter radar technique has been previously validated under controlled conditions in a gravity-driven falling solids stream, as described for the concentration in [15] and for the velocity in [12]. However, the ability of the radar-based technique measurements to characterize solids flows under conditions of industrial relevance has not been investigated.

The aim of the present work is to assess the applicability of the range-Doppler FMCW submillimeter wave radar technology for measurements of solids flows (concentration and velocity) under fluidized bed conditions. Towards this aim, experiments were carried out in a circulating fluidized bed (CFB) unit operated at room temperature. Measurements were performed at different fluidization velocities in order to cover the range of conditions from a bubbling to circulating regime, and while orienting the radar beam in the vertical and horizontal directions. The obtained profiles of solids concentrations and velocities were analyzed, to assess the suitability of this technique for studying solids flows. The present work does not aim at presenting a fluid dynamic study of a specific setup or regime, instead it aims at demonstrating and assessing the validity scope of this new radar technique.

2. Theory

The radar system used here operates in the FMCW pulse-Doppler mode, which makes it particularly useful for short-range (in the order of meters) applications [26]. In contrast to tomographic reconstruction techniques, radar diagnostics yield an inherently resolved measurement along the propagation line of the radar beam. The radar beam is a nearly cylindrical volume of small cross-section (which increases slightly in width with increasing distance from the radar antenna). When the radar beam is directed towards a suspension of solids, the transmitted radar signal is reflected back by the solids, and the signal power detected by

the radar antenna can be translated into a solids concentration, as it is a function of the projected cross-sectional area of the solids and the dielectric constant of the solids material. The position of the solid particles can be calculated from the round-trip delay time between the transmitted and reflected signals. Likewise, the frequency shift between successive pulses introduced by the movement of the solids is proportional to the solids velocity in the direction of propagation of the radar beam. In contrast to other radar systems that have been tested for the analysis of solids suspensions [13,14], the system employed here uses the same antenna for the transmitted and received signal, making it possible to perform measurements while pointing the beam in any direction. This provides additional flexibility to the measurement capabilities (e.g., by shifting the beam orientation, it becomes possible to measure three-dimensional fields).

2.1. Radar-based measurements of solids concentrations

Fig. 1 schematically illustrates a radar beam intersecting a cloud of solids. The antenna transmits sequences of linearly frequency-modulated pulses (n_p is the number of pulses, and *PRI* is the pulse repetition interval), and the reflections of these pulses from the solids are processed to calculate the distance relative to the antenna (range, R) and the velocity of the solids (v_d). The combination of the range resolution (ΔR) and cross-range resolution (defined by the width of the radar beam $d_{radar} = R\theta$, whereby θ is the angular beam width) yields the volume ($V_{radar} = \pi\Delta R(d_{radar}/2)^2$) in which the velocity and concentration of the solids, v_d and c_v, are measured. The radar range (or distance from the antenna) is proportional to the frequency difference (f_{IF}) induced by the round-trip delay time between the transmitted and reflected signals, expressed as: $R_R = f_{IF}c_0/(2\Delta f/\Delta t)$, where c_0 is the speed of light, and $\Delta f/\Delta t$ is the chirp rate of the frequency ramp.

The signal that is reflected back from the particles has a signal power P_r, which is expressed by the radar equation as follows [16]:

$$P_r = \frac{P_t G^2 \lambda^2 \sigma}{(4\pi)^3 R_R^4} \tag{1}$$

where P_t is the peak transmission power,G is the antenna gain, and σ is the back-scattering cross-section. This last term can be calculated as

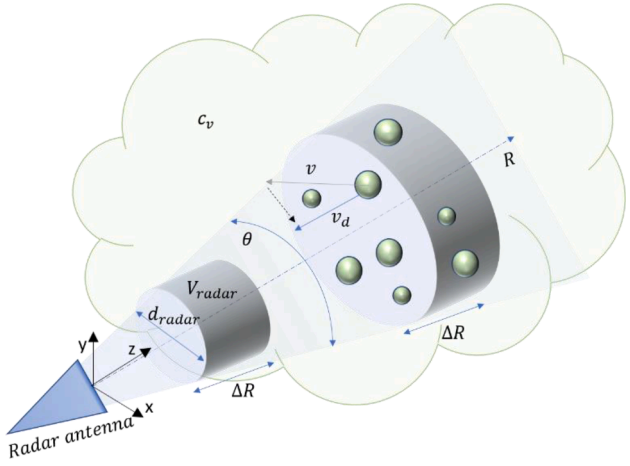

Fig. 1. Representation of a radar beam intersecting a gas-solids suspension. The radar beam transmitted by the antenna propagates along a straight line, and the cross-sectional area of the beam increases slightly (according to the angle Θ) with the distance from the antenna (called the range, R). The emitted signal power is scattered, absorbed (causing attenuation of the signal power with the range) and reflected by the solid particles. The reflected signal (also subjected to attenuation) processed to calculate the distance relative to the antenna. The Doppler shift is also assessed in the reflected signal to calculate the velocity of the solids. Source: [15].

$\sigma_b(r) = Q_b(r)\pi r^2$, for a single spherical particle of radius r, with Q_b being the back-scattering efficiency calculated according to Mie theory (for homogeneous spheres) [17]. In a cloud of similar particles, and under the assumption of single-scattering, the total back-scattering cross-section is according to Eq. (2):

$$\sigma_{b,tot} = n_{solids} V_{radar} \int_{r=r_{min}}^{r=r_{max}} f_{PSD}(r)\sigma_b(r)dr \tag{2}$$

where n_{solids} is the number of solids per unit volume, and f_{PSD} is the particle size distribution function.

Analogously, the total extinction cross-section is calculated as:

$$\sigma_{e,tot} = n_{solids} V_{radar} \int_{r=r_{min}}^{r=r_{max}} f_{PSD}(r)\sigma_e(r)dr \tag{3}$$

with Q_{ext} being the Mie extension efficiency, and assuming no multiple scattering. Q_b and Q_{ext} depend on the particle size, shape, and dielectric constant of the material. Regarding the effect of particle size on the scattering, two aspects must be considered. Firstly, as mentioned above, the validity of the single-scattering approximation (over multiple scattering) is supported by the use of sub-wavelength-sized solids at the concentration levels in this work [27]. Secondly, in the Mie theory used for the calculation of the scattering and the extinction coefficients (which corresponds to a solution of Maxwell's equations for the description of the scattering of a wave by a spherical particle), the scattering function depends (among other factors) on the particle size in a complex way [17,18]. A more extensive description of the signal processing and the assumptions made on scattering is presented in [Bohnmann et al., 2023].

All of the parameters specific to the radar set-up in Eq. (1) are collated, together with the hardware and signal processing gains and losses, into the factor K (found by calibration [15]), allowing the re-writing of Eq. (1) as Eq. (4):

$$P_r = \frac{K}{R_R^4} n_{solids} V_{radar} \int_{r=r_{min}}^{r=r_{max}} f_{PSD}(r)\sigma_b(r)dr \exp^{-2\int_0^l (f_{ext} n_{solids} \int_{r=r_{min}}^{r=r_{max}} f_{PSD}(r)\sigma_e(r)dr)dl} \tag{4}$$

where the exponential term accounts for the intensity of the radar beam that is reduced by the two-way attenuation caused by extinction (scattering and absorption) as the pulses travel back to the antenna, with *dl* being the range interval through which the beam has traveled. From the reflected signal power at the given position in the range (and for the corresponding beam width in that range), the number of solid particles is calculated. Based on this, the solids volume fraction can be calculated as:

$$c_v = n_{solids} V_{part} \tag{5}$$

where the average particle volume is given by:

$$V_{part} = \frac{4}{3}\pi \int_{r=r_{min}}^{r=r_{max}} f_{PSD}(r) r^3 dr \tag{6}$$

2.2. Radar-based measurement of solids velocities

The relative motion of the solids towards or away from the radar (in the direction of the beam propagation) induces a small frequency shift (f_d; Doppler shift) between successive pulses reflected back to the antenna. This phenomenon is used to derive the solids velocity in the direction of the beam propagation, as shown in Eq. (7):

$$v_d = f_d c_0/(2f_c) \tag{7}$$

where f_c is the center frequency of the radar. The maximal measurable velocity is $v_{max} = \pm c_0/(4f_C PRI)$, and the velocity resolution is $\Delta v = \frac{c_0}{2f_c n_p PRI}$, where n_p is the number of pulses that are coherently processed for one frame, and *PRI* is the pulse repetition interval. The calculation of velocity has been used in other FMCW radar applications [19], and was

validated for the current radar set-up in an earlier work [12]. Note that the solids velocity measured corresponds to the component of the velocity vector in the direction of the radar beam, e.g., z-component for vertical measurements.

3. Experimental set-up and data processing

3.1. The radar set-up

The settings for the radar set-up used in this work are summarized in Table 1. Further details regarding the radar hardware, signal processing and capacities of the set-up, are available elsewhere [12]. The maximal sampling frequency of the system f_s, is 250 MHz. However, for the purpose of this work, the sampling is performed at lower frequencies (62.5 Hz and 31.25 Hz) at different stages of the range-Doppler processing, in order to limit the volume of stored data. As a consequence, the range resolution ΔR_m is reduced by a factor of 8 and the range itself, R_m, is reduced by a factor of 32, which nonetheless ensures a range resolution of 5 mm, which is sufficiently height for the analysis of solids flows in a large unit. The execution time for the pulse train ($n_p \bullet PRI$) and the consecutive signal processing is set to 0.2 s (which means that the frame rate is set to 5 Hz or fps), so as to maintain reasonable data transfer rates. Real-life time resolution (30 Hz or fps) is possible, with the chosen frame rate being a compromise between the data transfer rate, range interval, velocity interval, and range and velocity resolution. The high center frequency and, thus, the short wavelength $\lambda = c_0/f_c$ of the radar (where c_0 is the speed of light) benefits the diffraction-limited cross-range resolution $\Delta d \approx \lambda R_R/D$ (where D is the diameter of the radar antenna) and increases the sensitivity to detect small particles. The range resolution is $\Delta R \approx c_0/(2BW)$, where BW is the bandwidth of the transmitted radar signal. Thus, the radar enables the characterization of volumes in the order of cubic centimeters. For the experiments reported here, the width of the radar beam inside the fluidized bed was in the range of 40–60 mm (experimental determination of the radar beam width is presented in [15]).

3.2. The fluidized bed riser

In the present work, a CFB operated under ambient conditions was used (the unit being designed to mimic a fluidized bed boiler). The main components of the unit are visualized in Fig. 2 (for details, see [20]). The riser outlet is connected to a cyclone that separates the solids from the gas. The separated solids pass through the downcomer into a loop seal. The downcomer and loop seal provide the pressure difference required to reinject the solids into the main chamber. The riser of the model (i.e., the furnace in a full-scale unit) is built of acrylic glass to allow visual inspection of the solids flow. The riser has vertical walls through its entire height and a horizontal roof. The air is supplied by two inlet fans, which together with a suction fan at the outlet ensure a pressure below atmospheric pressure for the whole loop of solids, in order to prevent solids leakage. The air distributor is made up of two perforated plates separated by a fine mesh. A hose filter is installed before the suction fan to collect the small fraction (<1%) of solids that cannot be separated in the cyclone. Pressure taps are installed along the riser height (at 15 different positions), in the air plenum, the cyclone outlet, the downcomer, and the particle filter after the cyclone. The pressure measurements can be used to determine the average concentrations of solids, $\rho_s(1-\varepsilon_g)$, where $\varepsilon_g$is derived (neglecting acceleration effects [21]) from Eq. (8):

$$\Delta P = \left((\rho_s - \rho_g)(1-\varepsilon_g) + \rho_g \varepsilon_g\right) g \Delta h \tag{8}$$

In the present study, the bed material consists of glass beads with a mean particle size of 106 μm (d_{10} = 75 μm, d_{90} = 160 μm), PSD as presented in Fig. 3 (obtained by laser diffraction using the Mastersizer 3000, Malvern Panalytical), and a particle density of 2,486 kg/m^3 (density values obtain by Hg porosimetry using the AutoPore III, Micromeritics). The minimum fluidization velocity and terminal velocity of the particles are 0.013 m/s and 0.64 m/s, respectively.

Table 1
Radar parameters used in this work.

Center frequency	f_C	340 GHz
Bandwidth	BW	19.2 GHz
Raw range resolution	ΔR	5 mm
Chirp rate	$\Delta f/\Delta t$	777.8 MHz/μs
Number of pulses	n_p	128
Pulse repetition interval	PRI	48 μs
Maximal sampling frequency	f_s	250 MHz

3.3. Assembly

Radar measurements were performed by orienting the radar beam both horizontally and vertically. For the horizontal measurements, a section of the lateral wall proximal to the riser outlet was replaced with a HDPE (high-density polyethylene) plate, and the radar beam was pointed horizontally towards the unit, as presented in Fig. 4. For the vertical measurements, the riser roof was replaced with a HDPE plate, as shown in Fig. 5. HDPE was used because this material attenuates a considerably smaller faction of the radar power compared to acrylic plastic (used in the riser walls), i.e., the radar beam can penetrate the solids suspension with higher power and the reflected signal that is returned is stronger, so it can be detected by the antenna. Given the spatial restrictions, it was not possible to direct the radar beam directly into the unit, so instead a metallic flat mirror was used to redirect the beam in the desired direction (perpendicular to the corresponding HDPE plate), as illustrated in Figs. 4 and 5.

3.4. Data presentation

The reflected radar signal containing the velocity and power data along the sight-line can be represented in range-velocity-signal power maps. Examples of such maps for a set of different measurements are presented in Fig. 6 (the results in this figure are illustrative; the systematic presentation of results and corresponding discussion can be found in Section 4). Static reflections (resulting from the walls) are removed by filtering out the signal reflected at velocity of zero. Note that the range zero corresponds to the antenna itself, while the fluidized bed chamber has range limits at 0.4 m for the roof and 3.5 m for the air distributor. In the range-velocity-signal power maps, the range axis spans within: $R_m = f_{mix}c_0/(2\Delta f/\Delta t) \pm f_s c_0/(4\Delta f/\Delta t)$, where f_s is the sampling frequency of the analog-to-digital converter, and f_{mix} is the digital mixing frequency. The range-bin spacing corresponds to the spatial resolution and is given by: $\Delta R_m = f_s c_0/(2n_s\frac{\Delta f}{\Delta t})$, where n_s is the number of samples taken per pulse, when converting the signal from analog to digital. The velocity axis covers the interval: $v_m = \pm c_0 PRF/(4f_C)$, where $PRF = 1/PRI$ is the pulse-repetition frequency. The velocity-bin spacing, corresponding to the velocity resolution, is: $\Delta v_m = 2v_m/n_p$, where n_p is the number of pulses that are coherently integrated. The range and velocity intervals can easily be adjusted by changing the radar parameters of $\Delta f/\Delta t$, and PRF and n_p, respectively.

Note that the color maps in Fig. 6 show how the penetration of the radar beam is reduced as the fluidization velocity increases (and, thus, the solids concentration in the freeboard). This is an indication that the higher the solids concentration the more attenuated will be the signal power. It can also be seen that for each position along the range, there is a specific distribution of the measured velocities. The data presented in this work are averaged over a period of 15 s. This period was selected because it provides stable averages and file sizes adequate for processing. Fig. 7 exemplifies, for a selected experiment, the difference between single frames toguether with a range-velocity-signal power map plotted for data averaged over 15 s. Note that the measurement captures the

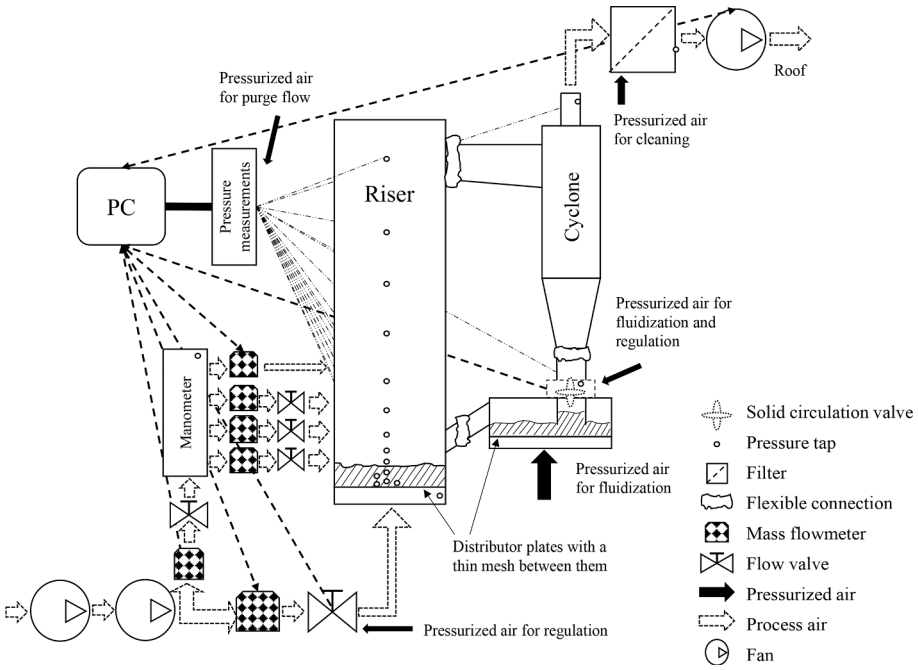

Fig. 2. Schematic of the circulating fluidized bed unit used. Source: [20].

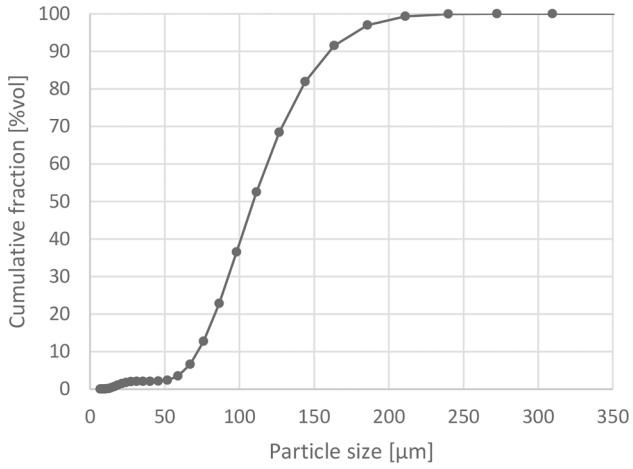

Fig. 3. Particle size distribution of the bed material (glass beads) used in the experiments.

fluctuations of velocity and concentration occurring between frames (with a time step here set to 0.2 s). The noise performance of the acquired signal was studied in a previous work [12] concluding that regardless of the radar settings, the noise is uncorrelated with the radar signal, and therefore not dependent on the integration time.

4. Results and discussion

4.1. Solids velocity measurements

Fig. 8 shows examples of profiles of time-averaged solids mean velocities obtained from the radar measurements, with the beam being oriented both vertically and horizontally for different fluidization velocities. Negative velocity values indicate movement of the solid particles towards the antenna, i.e., upwards for the vertical measurements (Fig. 8a) and towards the riser outlet wall for the horizontal measurements (Fig. 8, b and c). The range indicates the distance from the radar antenna, i.e., vertical and increasing from the top to the bottom of the riser, for the measurements where the radar penetrated from the top (Fig. 8a), and horizontal and increasing from the back to the front wall of the riser for the experiments where the radar penetrated through the window in the back side of the riser (Fig. 8, b and c). The highly oscillating profiles indicate strong intrinsic variations in solids velocity, which are not overcome by the integration time used in this study. A statistical analysis of velocity variations as function of the number of integrated frames will be subject of further investigations.

The profiles of the time-averaged vertical solids mean velocities (Fig. 8a) reveal the changes in the solids velocity at different positions in the height of the riser as the fluidization velocity increases, that is, as the operation progressively changes from bubbling to circulating conditions. The transport velocity of the bed material estimated for its mean particle size is 0.64 m/s. It should be noted that the velocity profile gives the time-averaged velocity over a nearly cylindrical volume (4–6 cm in diameter), i.e., what is covered by the radar beam and only in the direction in which the beam is pointed (strictly vertically in this case). Thus, the results shown in Fig. 8a cannot be assumed to be the same over the entire cross-section.

The negative average velocity values observed along most of the vertical center line indicate a net ascending flow of solids in this region, which increases in magnitude as the fluidization velocity increases. Only at the lowest part of the riser (in the strongly back-mixing bottom region) and only for low fluidization velocities (bubbling fluidization regime) does the descending movement of particles dominate for the portion of the cross-section sampled by the beam. This means that, on average, there is a local net down-flow of solids, typical of the gulf-stream solids mixing pattern seen in dense bottom beds [22,23]. In particular, at high fluidization velocities (see, for instance, the profiles for 1.0 m/s and 1.2 m/s in Fig. 8a), it is also observed that the mean solids velocity increases with height, which can be attributed to back-mixing effects, i.e., only smaller particles continue in the upwards flow, thereby yielding a decrease in the net terminal velocity and an increase in the net upwards velocity. Alternatively, the constant back-mixing at the walls can decrease the concentration of solids in the core and allows the achievement of higher velocities in that region. Additional measurements made at different positions over the cross-section should facilitate a more-detailed analysis. For high fluidization velocities, the prevalence of descending particles is also observed just

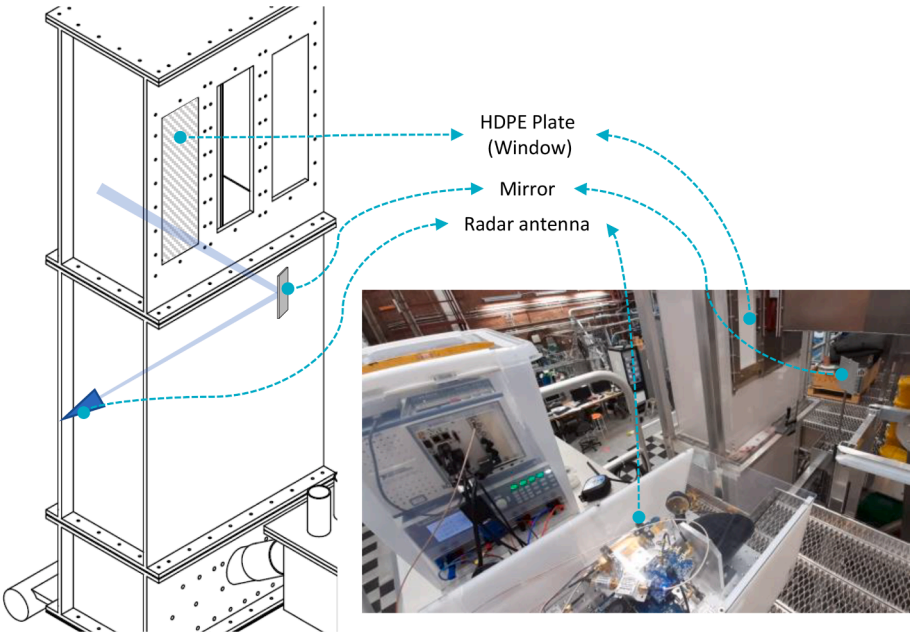

Fig. 4. Schematic of the experimental assembly used for horizontal measurements, indicating the relative position of the radar antenna.

position of the radar antenna.

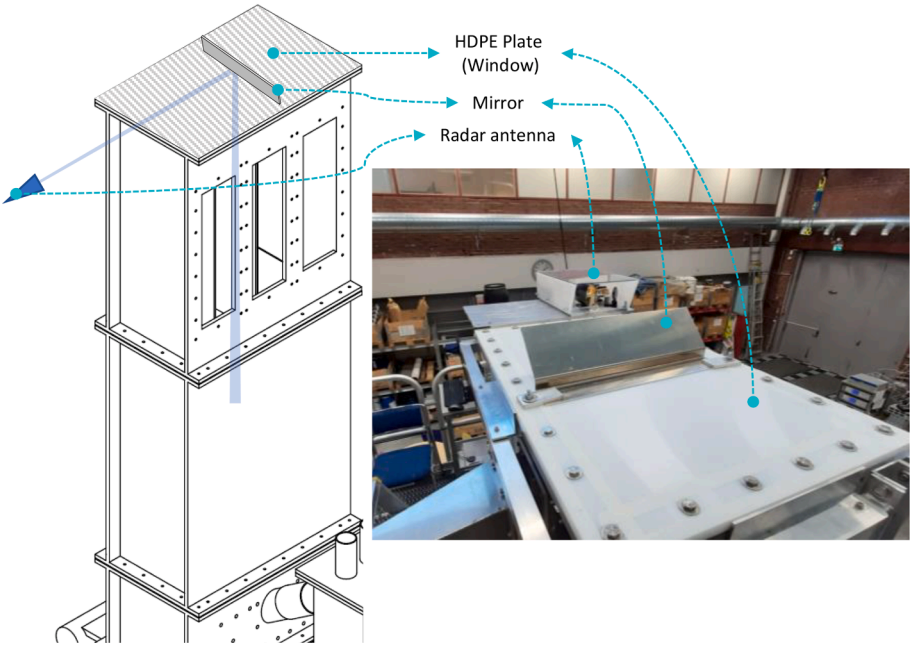

Fig. 5. Schematic of the experimental assembly used for vertical measurements, indicating the relative position of the radar antenna.

below the riser outlet.

The horizontal profiles of the time-averaged solids velocities measured at distances of 0.4 m and 0.7 m from the top (Fig. 8, b and c) show that the magnitude of the average horizontal velocity increases with fluidization velocity. Furthermore, the dominant negative velocities show that for all the tested conditions there is, at both heights (i.e., 0.4 m and 0.7 m from the top), a net movement of particles towards the riser outlet wall (located approximately 0.4 m from the roof). Note that for the height level corresponding to the riser exit, Fig. 8a indicates a mean solids vertical velocity that is closer to zero, meaning that there is a balance between the ascendent and descendent solids flows. For fluidization velocities $\geq$ 0.7 m/s, a flow structure can be inferred (from the s-shaped profile), in which the mean velocity in the first half of the unit (closer to the outlet) approaches zero, suggesting a comparatively larger fraction of particles moving towards the center. Furthermore, as the fluidization velocity is increased, the horizontal velocity of the particles close to the wall opposite the outlet (first few centimeters in Fig. 8, b and c, from right to left) changes from about zero to positive values, implying a net lateral transfer of solids from the riser core region towards that wall. Comparing the data in Fig. 8, b and c, it appears that the qualitative trends are maintained, although at a lower height much lower mean velocities are observed, suggesting a less-dominant lateral

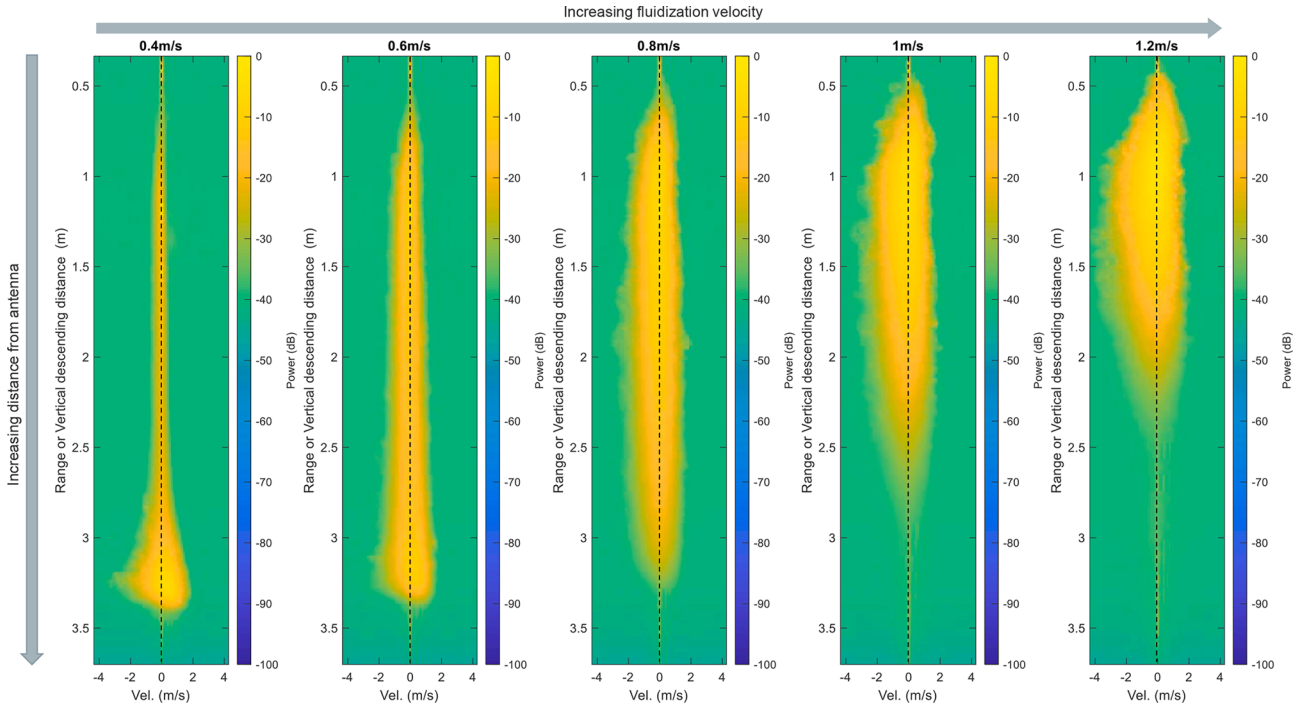

Fig. 6. Examples of the range-velocity-signal power maps obtained at different fluidization velocities with a solids inventory of 120 kg. The radar beam is oriented in the vertical direction along the riser centerline, entering from the top. The *x*-axis shows the magnitude of the solids velocity component in the direction of the radar propagation (vertical in this case), where positive values indicate descendent movement and negative values indicate ascendent movement. The *y*-axis shows the range (distance from the antenna); here, only the window corresponding to the riser is shown (riser roof at ≈0.4 m, air distributor at ≈3.5 m). The color scale indicates the signal power (or reflection intensity) received from the given range and velocity. The presented data-points correspond to average values calculated over 15 s.

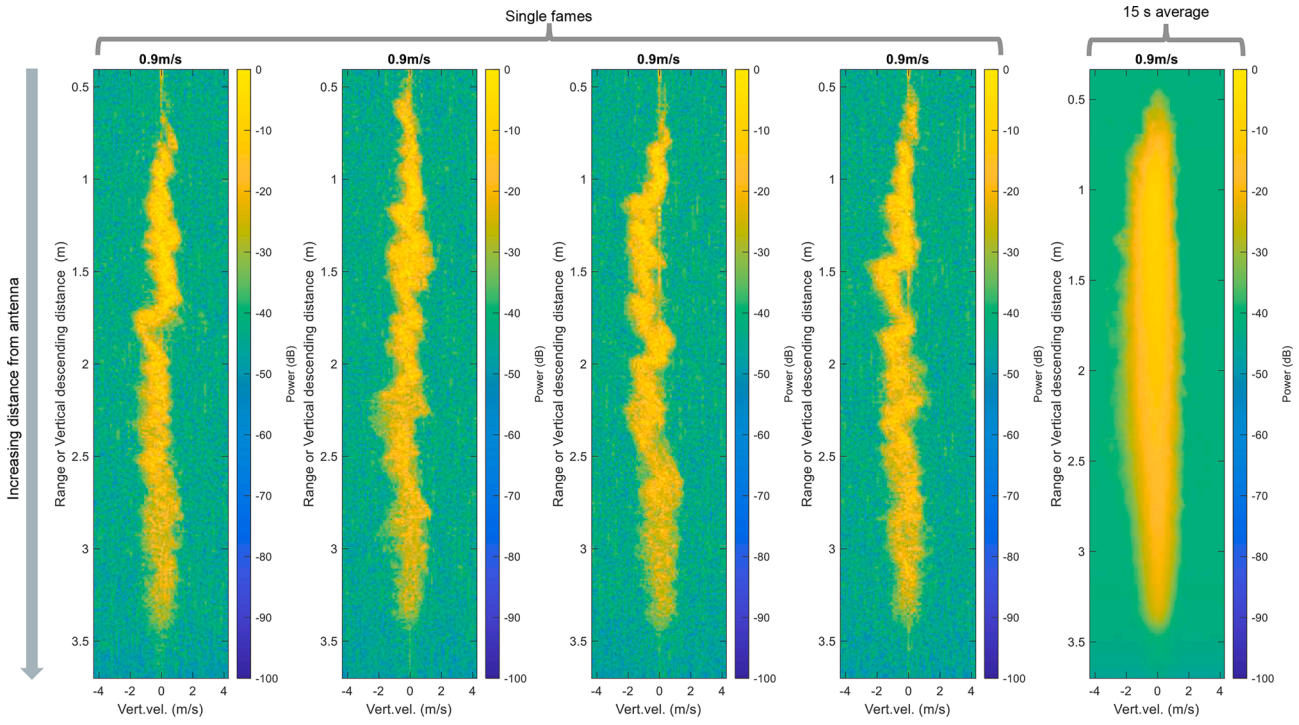

Fig. 7. Example of the range-velocity-signal power maps obtained at a fluidization velocity of 0.9 m/s with a solids inventory of 60 kg. The first four maps from the left correspond to single frames, and the right-most map shows the data averaged over 15 s. The radar beam is oriented in the vertical direction along the riser centerline, entering from the top. The *x*-axis shows the magnitude of the solids velocity component in the direction of the radar propagation (vertical in this case), where positive values indicate descendent movement and negative values indicate ascendent movement. The *y*-axis shows the range (distance from the antenna); here, only the window corresponding to the riser is shown (riser roof at ≈0.4 m, air distributor at ≈3.5 m). The color scale indicates the signal power (or reflection intensity) received for the given range and velocity.

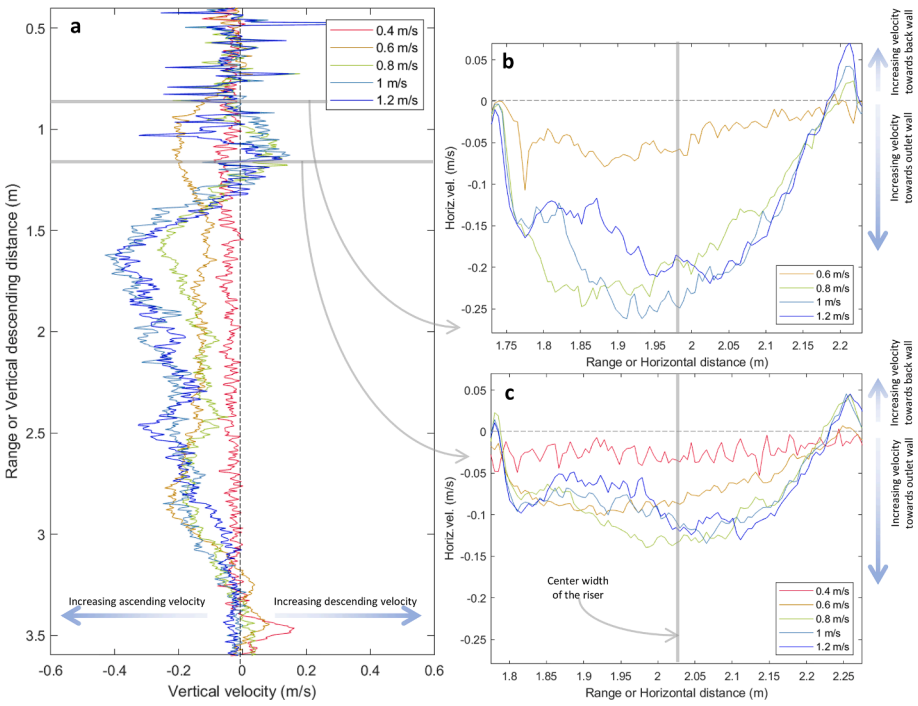

Fig. 8. Time-averaged solids velocities measured at different fluidization velocities and using 60 kg of inventory. a. Measurements along the center vertical line of the riser (range values in *y*-axis: riser roof at ≈0.4 m, air distributor at ≈3.5 m). Negative velocities correspond to ascendent movement of solids. The gray lines indicate the approximate positions of the radar beam for the horizontal measurements. b and c. Measurements along the horizontal lines of the bed located at 0.4 m and 0.7 m from the riser roof, respectively. Negative velocities correspond to movement of the solids towards the rear wall of the riser (where the outlet is located). The gray lines indicate the approximate positions of the radar beam for the vertical measurements.

movement towards the outlet wall.

The signal strength differentiates between solids with different velocities and, thus, between the shares of particles (relative to the total volume of solid particles found at the given positions) traveling at a given velocity in a given direction. Fig. 9 shows examples of the distributions of vertical solids velocities at seven different heights in the riser for a fluidization velocity of 0.8 m/s and a bed inventory of 120 kg. It is evident that at all positions both ascending and descending particles can be detected, although the shares of the different velocities change with the vertical position in the bed.: Note also that profiles, such as those presented in Fig. 8 are constructed with the mean values extracted from the distributions of velocities at the different positions in the range (every 5 mm).

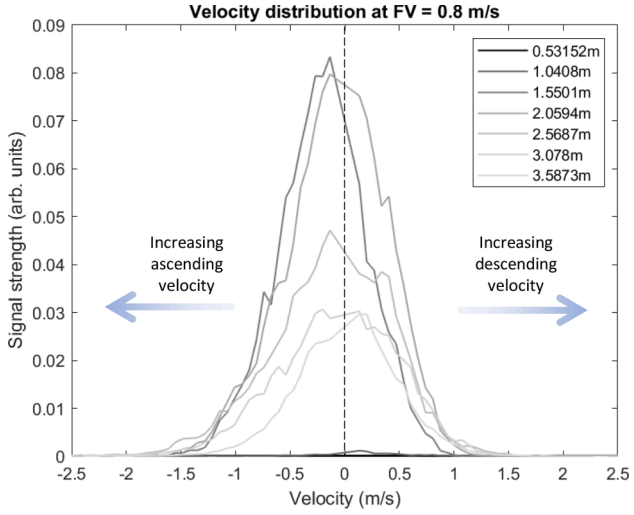

Fig. 9. Time-averaged measured solids velocities at different heights in the bed, presented as distributions of the solids vertical velocity. Measurements were performed with 120 kg of inventory and a fluidization velocity of 0.8 m/s, with the radar aligned to the center of the horizontal cross-section of the unit. Distances reported are from the radar antenna (an increasing value means a lower height level inside the bed).

4.2. Solids concentration measurements

Before analyzing the concentration profiles obtained, the extent of signal attenuation (caused by absorption and scattering of both the transmitted and reflected signals), and thus the ability of the radar beam to penetrate the solids suspension, was assessed. This was done by comparing the power signal along the sight-line of the radar to the background signal level for experiments performed in the vertical direction. Fig. 10 shows the comparison of the reflected signals from measurements performed at different velocities (yielding different concentration profiles) with the signal acquired from the empty unit (background measurement). It is clear that for sufficiently long distances from the radar antenna, the reflected signal power eventually decreases to the background value. In other words, the power emitted from the antenna is attenuated to such an extent that no effective reflections can be read from those positions. These maximum penetration distances depend on the number of particles encountered by the beam along its propagation line (this is, the concentration integrated along the sight-line). For the exemplifying cases presented in Fig. 10, it can be seen that the maximum penetration distance is shortened as the gas velocity is increased and, thus, the concentration of the solids suspension in the top section of the riser increases (as does the number of particles encountered by the radar beam). Solid particles in a CFB typically become distributed along the riser height, yielding a dense bed in the bottom region, followed by a splash zone above which there is a lean region (sometimes referred to as the 'transportation region' with mainly upward-moving solids across the core region [24,25]. The higher the gas velocity, the higher the solids concentration in the upper part of the riser and the lower the concentrations in the bottom bed and the splash zone. Considering this, for each concentration measurement, the valid range interval (corresponding to a penetration length) is selected as that within which the reflected signal is higher than the background level. Thus, the power signal data from range locations beyond the penetration length are discarded. It should be noted that the progressive decay of the signal power is expected as a product of absorption and scattering, and the conversion of signal power to concentration considers the two-way attenuation. Thus, a low signal level is not a reason to discard a measurement but it is necessary to confirm that the received signal is higher

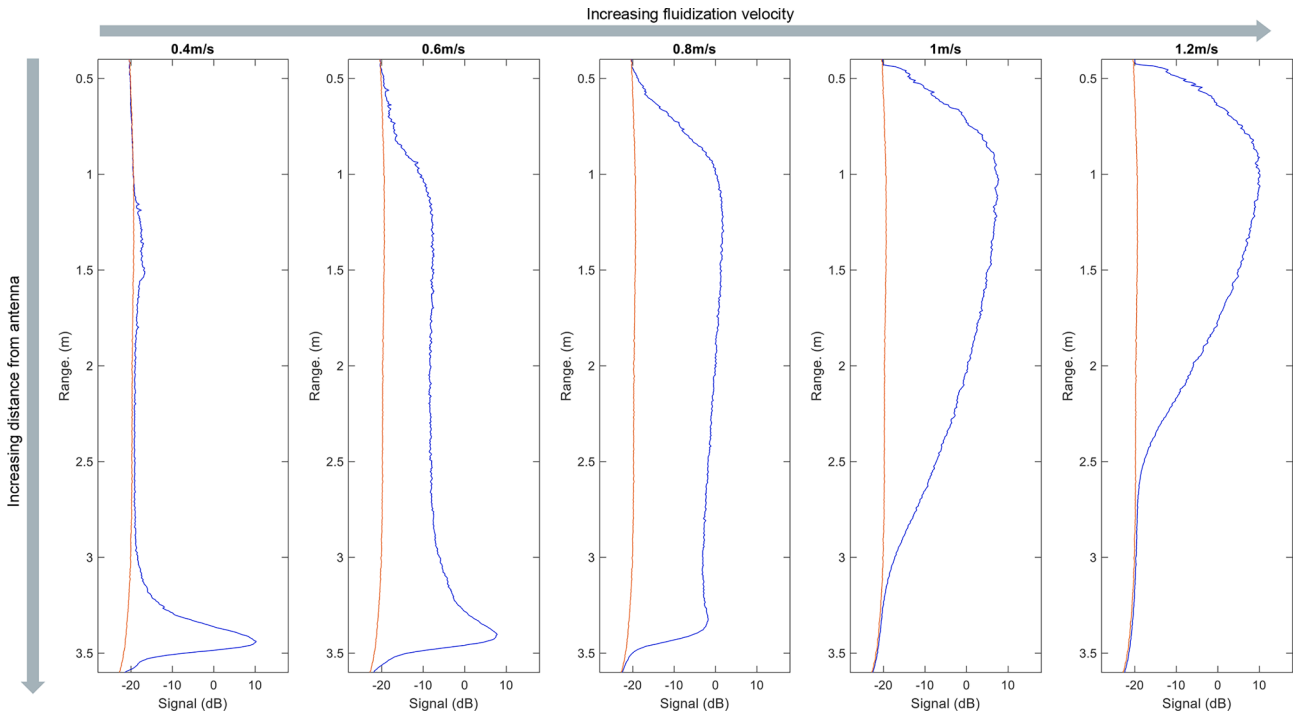

Fig. 10. Example of the signal power decay caused by absorption and scattering. Comparison of the background reflection (red line) with the power signal obtained for measurements shows that the signal power eventually drops to the level of the background, after which point, the signal power is no longer applicable for the determination of solids concentrations. The measurements presented here were obtained along the center vertical line of the riser at different fluidization velocities with 60 kg of inventory.

than the background level.

The solids volume concentration profiles obtained by applying Eq. (4) to the signal power levels acquired from positions along the vertical center line of the unit are presented in Fig. 11 for different fluidization velocities. Note that the penetration length changes as the concentration of solids increases in the top section of the riser. In the profiles presented in Fig. 11a, for velocities < 0.8 m/s, the radar beam penetrates down to the dense zone (i.e., almost 3 m), while it penetrates only slightly

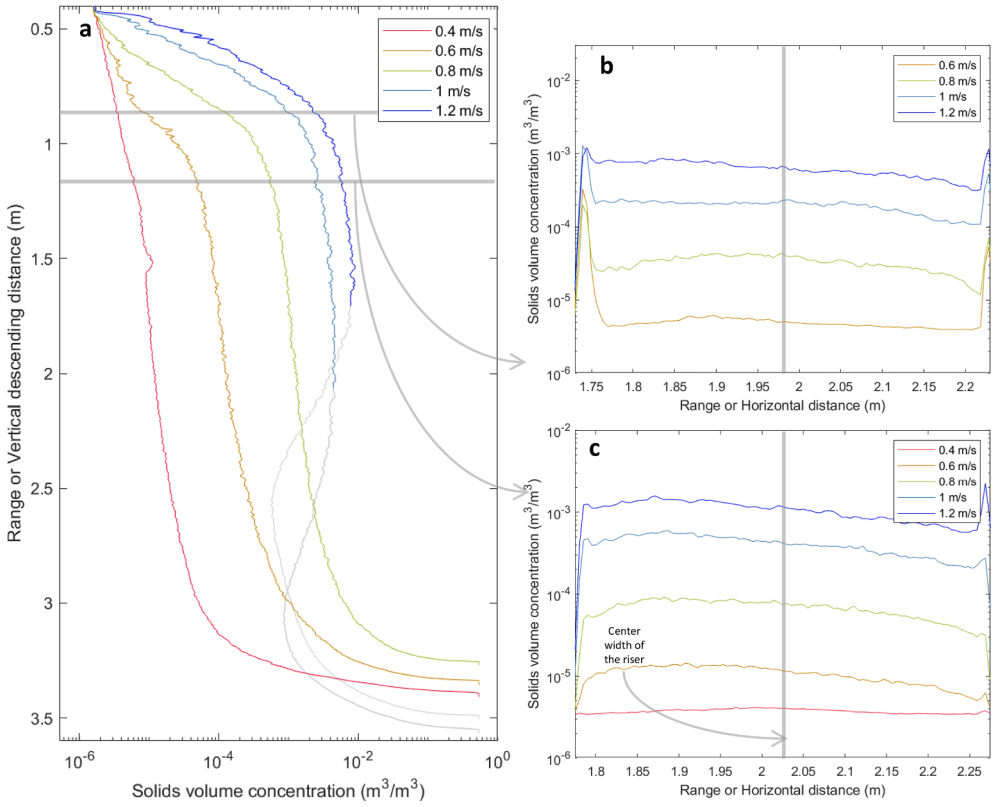

Fig. 11. Solids concentration profiles calculated as described in Section 2, for different fluidization velocities with 60 kg of inventory. a Measurements along the center vertical line of the riser. The gray lines indicate the approximate positions of the radar beam for the horizontal measurements. b and c. Measurements conducted along the horizontal lines located 0.4 m and 0.7 m from the riser roof. The gray lines indicate the approximate positions of the radar beam for the vertical measurements.

beyond 2.0 m and 1.5 m for fluidization velocities of 1.0 m/s and 1.2 m/s, respectively. In general, solids concentrations of up to 10^{-2} m^3/m^3 could be measured at the top of the unit, while concentrations higher than to 10^{-1} m^3/m^3 were measured in the dense bed. For the measurement of very high concentrations, such as those present in dense beds, consideration of multiple scattering in the processing of the data might be necessary. The vertical profiles of solids concentrations in the riser exhibit a shape that is very similar to the expected one: a steep decrease in solids concentration in the lower part of the riser (bed and splash zone), followed by a less-steep decrease along most of the riser height (transport zone), and topped by a strong decrease in the vicinity of the riser roof. Previous studies have described these concentration decays as exponential [24], which would yield straight lines in Fig. 11a; this specific characteristic is evident in some sections of the profiles. As the gas velocity increases further, a higher concentration of solids is observed in the upper part of the riser, which causes attenuation of the signal and, thereby, limits the signal penetration. To extend the scope to higher penetration lengths at higher solids concentrations, modifications to the hardware and software may be considered.

Fig. 11, b and c give the corresponding horizontal solids concentration profiles from measurements made at distances of 0.4 m and 0.7 m from the riser roof. The results obtained from the measurements performed horizontally show an increase in the solids concentration with increasing fluidization velocity. The average concentrations are similar to the concentrations observed at the corresponding heights with the vertical measurements. It should be noted that the vertical measurements were performed at the center of the cross-section, while the horizontal measurements were performed on one side of the unit (see Figs. 4 and 5).

Fig. 12 compares the vertical profiles of the solids concentrations obtained from radar measurements (solid lines) to the concentration values derived from pressure measurements (empty square markers, see Eq. (6)), and their corresponding fitting to a theoretical model (dashed line). Since the radar measurements are local (few cubic centimeters) and the pressure drop measurements can only report cross-sectional averaged concentrations, a quantitative comparison cannot be undertaken. The theoretical model, which consists of the sum of two exponential decays, was originally presented by Johnsson and Leckner [24] and further developed and validated applying extensive data from hot and cold units by Djerf and coworkers [28]. The model fitting helps to provide a consistent, pressure-derived concentration profile for the comparison, which is especially needed for very low concentrations, for which the small pressure differences and limited accuracy of pressure transducers yield inaccurate values (recognized as a major drawback associated with the use of pressure measurements for diagnosing CFB flows). These inconsistent concentration values were removed before fitting the model, but their position is represented in the figure by black solid filled markers at the left edge of the plotting area. Note that for low fluidization velocities, only one exponential decay is calculated (for the lower section of the riser), since under those conditions, the transport of solids is negligible. In the top section of the unit, it can be seen that once the solids concentration reach a value high enough to be measurable with the pressure transducer the pressure drop and the radar measurements show satisfactory agreement.

It can be seen in Fig. 12 that the radar technique has a very high level of sensitivity, being able to describe the concentration changes in the riser top, i.e., the solids-leaner region, which is not possible using pressure drop measurements. In the denser bottom region, it can be seen that the concentration values obtained with radar agree to a large extent with those extracted from pressure measurements. However, the radar power is strongly attenuated as it penetrates the dense zone.

5. Conclusions

Presented herein are the first experiences of measurements carried out in a CFB reactor applying the FMCW pulse-Doppler radar technology. We conclude that the radar measurements are able to provide non-intrusive measurements of solids concentrations and solids velocities,

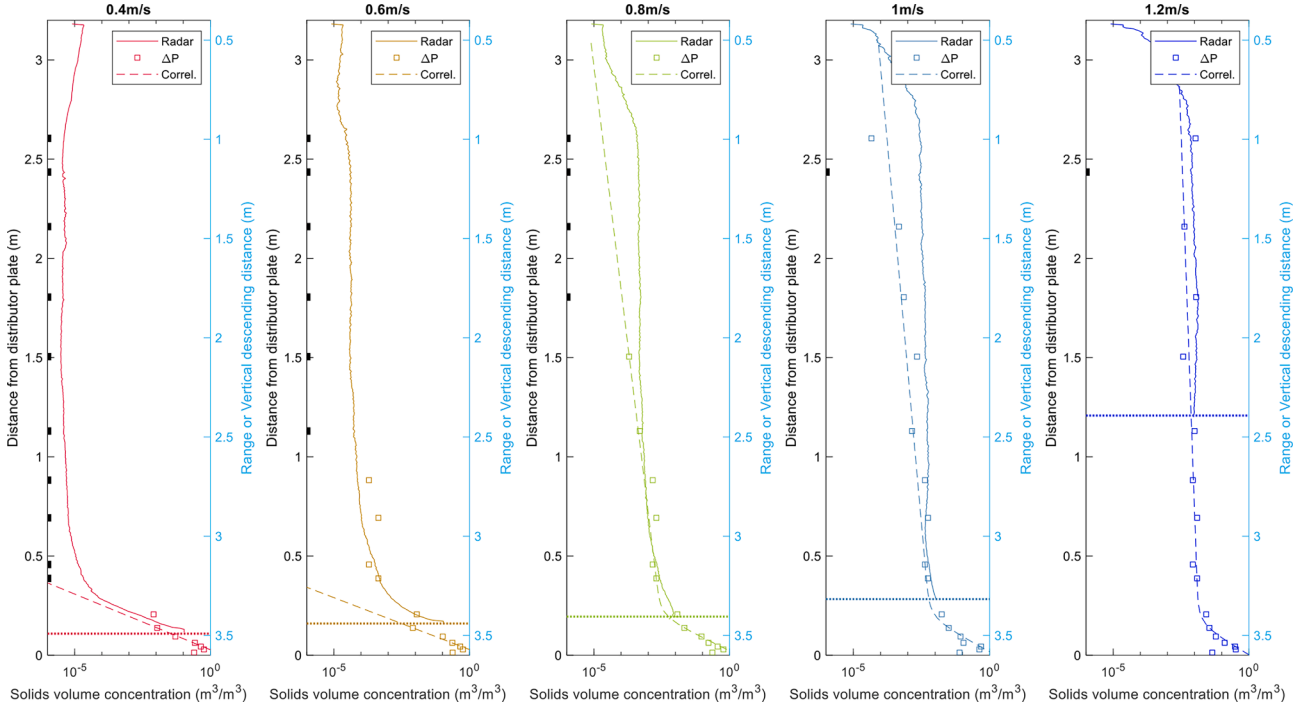

Fig. 12. Comparison of the concentration profiles obtained from radar measurements in the vertical direction along the riser centerline (solid line), pressure differences (from pressure taps on the wall of the unit, presented as empty markers), and a theoretical model consisting of the sum of two exponential decays and fitted to the pressure data (dashed line). Pressure-derived concentrations become inconsistent as the pressure difference approaches zero, such values were intentionally removed but their position is represented by black solid filled markers. The comparison is presented for different fluidization velocities with a solids inventory of 120 kg.

resolved in space and time.

Profiles of solids velocities and the distribution of solids velocities were successfully measured from the Doppler effect in the vertical and horizontal directions. The concentration profiles acquired capture the impacts on the solids concentrations and velocities of changes to the fluidization velocity. For vertical measurements, limitations regarding the penetration of the radar beam could be observed at high fluidization velocities, for which the solids concentration integrated along the sight-line of the beam rapidly increases due to the higher concentrations in the upper section of the riser, which cause the signal power to be fully attenuated before it reaches the lower section of the riser. The radar-based measurement appears especially suitable for low concentrations of solids ($<5{\cdot}10^{-3}$ m^3/m^3, approximately), for which it provides more-consistent measurements of the solids concentration than those derived from pressure transducers. Satisfactory quantitative agreement is achieved with pressure-derived concentration profiles, for solids volume fractions between $5{\cdot}10^{-3}$ m^3/m^3 and $1{\cdot}10^{-1}$ m^3/m^3. Solids concentrations $\geq 1{\cdot}10^{-1}$ m^3/m^3, such as those found in the dense zone in the lower section of the riser, strongly reduce the penetration depth of the beam and presumably require a revision of the single-scattering assumption. Moreover, it must be stressed that the comparison with pressure-based concentration measurements is only indicative, since the radar measurements are more local than the cross-sectional average concentrations obtained from the pressure drop measurements.

In summary, the radar technique applied in this work can provide important information for detailed characterization of the solids flows in fluidized beds, while offering fundamental advantages in terms of its non-intrusive nature and its high spatial and temporal resolutions, conferring the possibility to determine both the solids velocity and concentration with reasonably high penetration. Nonetheless, further work is required to increase the level of penetration at high solids concentrations, as well as to revise the assumption regarding single-scattering. Further refinements of the technique and the radar setup are needed to eliminate the influence of static reflections and to narrow the radar beam.

CRediT authorship contribution statement

Diana Carolina Guío-Pérez: Conceptualization, Methodology, Formal analysis, Investigation, Writing – original draft. **Marlene Bonmann:** Conceptualization, Methodology, Formal analysis, Investigation, Writing – review & editing. **Tomas Bryllert:** Conceptualization, Formal analysis, Writing – review & editing, Funding acquisition. **Martin Seemann:** Writing – review & editing. **Jan Stake:** Supervision. **Filip Johnsson:** Writing – review & editing, Funding acquisition. **David Pallarès:** Conceptualization, Writing – review & editing, Supervision.

Declaration of Competing Interest

The authors declare that they have no known competing financial interests or personal relationships that could have appeared to influence the work reported in this paper.

Data availability

Data will be made available on request.

Aknowledgments

Financial support from Svensk Strategisk Forskning and the Chalmers Energy Area of Advance is acknowledged.

References

[1] Van Ommen JR, Sasic S, van der Schaaf J, Gheorghiu S, Johnsson F, Coppens M-O. Time-series analysis of pressure fluctuations in gas–solid fluidized beds – A review. Int J Multiph Flow 2011;37(5):403–28. https://doi.org/10.1016/j.ijmultiphaseflow.2010.12.007.
[2] Van Ommen R, van der Schaaf J, Schouten J, van Wachem B, Coppens MO, van den Bleek CM. Optimal placement of probes for dynamic pressure measurements in large-scale fluidized beds. Powder Technol 2004;139(3):264–76.
[3] Zhang W, Johnsson F, Leckner B. Momentum probe and sampling probe for measurement of particle flow properties in CFB boilers. Chem Eng Sci 1997;52(4):497–509.
[4] Wiesendorf V, Werther J. Capacitance probes for solids concentration and velocity measurements in industrial fluidized bed reactors. Powder Technol 2000;110(1–2):143–57.
[5] Xu Y, Li T, Lu L, Gao X, Tebianian S, Grace JR, et al. Development and confirmation of a simple procedure to measure solids distribution in fluidized beds using tracer particles. Chem Eng Sci 2020;217:115501.
[6] Wang H, Yang W. Application of electrical capacitance tomography in pharmaceutical fluidized beds – A review. Chem Eng Sci 2021;231:116236. https://doi.org/10.1016/j.ces.2020.116236.
[7] Wang H, Yang W. Application of electrical capacitance tomography in circulating fluidized beds – A review. Appl Therm Eng 2020;176:115311. https://doi.org/10.1016/j.applthermaleng.2020.115311.
[8] Peltola J, Karvonen L, Elfvengren J, Kolehmainen J, Kallio S, Pallarès D, Johnsson F, Measurement of solids velocity and concentration in a large cold CFB model. 11th Int. Conf. on Fluidized Bed Technology (2014).
[9] Cooper KB, Dengler RJ, Llombart N, Bryllert T, Chattopadhyay G, Schlecht E, et al. Penetrating 3-D Imaging at 4- and 25-m Range Using a Submillimeter-Wave Radar. IEEE Trans Microw Theory Tech 2008;56:2771–8.
[10] Luukanen A, Grönberg L, Grönholm M, Lappalainen P, Leivo M, Rautiainen A, et al. Real-time passive terahertz imaging system for standoff concealed weapons imaging. Proc SPIE 2010;7670.
[11] Bryllert T, Submillimeter wave diode transceivers, International Conference on Infrared, Millimeter, and Terahertz Waves, IRMMW-THz. (2014).
[12] Bryllert, T, Bonmann M, Stake J, A Submillimeter-Wave FMCW Pulse-Doppler Radar to Characterize the Dynamics of Particle Clouds, IEEE Transactions on Terahertz Science and Technology. Vol. 13. (2023). https://arxiv.org/pdf/2301.00558.pdf.
[13] Reinhardt A, Teplyuk A, Knochel R, Höft M, Remote measurement of particle streams with a multistatic dual frequency millimeter wave radar sensor, IEEE/MTT-S International Microwave Symposium – IMS (2018a) p. 127-130.
[14] Reinhardt A, Teplyuk A, Knöchel R, Höft M, Size determination in particle streams using a multistatic dual frequency millimeter wave radar, 15th European Radar Conference (2018b) p. 413-416.
[15] Bonmann M, Guío-Pérez DC, Bryllert T, Pallarès D, Seemann M, Johnsson F, Stake J. A submillimetre wave range-Doppler radar as a diagnostic tool for gas-solids systems – solids concentration measurements. (2022, manuscript).
[16] Stimson GW, Griffiths HD, Baker CJ, Adamy D. Stimson's Introduction to airborne radar. 3rd Edition. Institution of Engineering and Technology; 2014.
[17] Bohren CF, Huffman DR. Absorption and scattering of light by small particles. New York, NY: John Wiley; 1983.
[18] Michael I, Mishchenko, Liu Li, Videen Gorden. Conditions of applicability of the single-scattering approximation. Optica Express 2007;15:7522–7.
[19] Alyasmi R, FMCW radar – Signal processing and parameter estimation, Scientific report, (2002) Swedish defence research agency, FOI. Sensor technology, Sweden.
[20] Djerf T, Pallarès D, Johnsson F. Bottom-bed fluid dynamics: Influence on solids entrainment. Fuel Process Technol 2018;173:112–8.
[21] Sasic S, Leckner B, Johnsson F. Characterization of fluid dynamics of fluidized beds by analysis of pressure fluctuations. Prog Energy Combust Sci 2007;33(5):453–96.
[22] Agarwal P. The residence phase of active particles in fluidized beds of smaller inert particles. Chem Eng Sci 1987;42(10):2481–3.
[23] Pallarès D, Johnsson F. A novel technique for particle tracking in cold 2-dimensional fluidized beds—simulating fuel dispersion. Chem Eng Sci 2006;61(8):2710–20. https://doi.org/10.1016/j.ces.2005.11.030.
[24] Johnsson, F., & Leckner, B. (1995). Vertical distribution of solids in a CFB-furnace. 13th Int. Conf. on Fluidized Bed Combustion. Orlando (Florida, USA).
[25] Zhang W, Johnsson F, Leckner B. Fluid-dynamic boundary layers in CFB boilers. Chem Eng Sci 1995;50(2):201–10. https://doi.org/10.1016/0009-2509(94)00222-D.
[26] Kärnfelt C, Péden A, Bazzi A, El Haj Shhadé G, Abbas M, Chonavel T, 77 GHz ACC radar simulation platform, *9th International Conference on Intelligent Transport Systems Telecommunications, (ITST)*, (2009) p. 209-214.
[27] Mishchenko MI, Liu L, Videen G. Conditions of applicability of the single-scattering approximation. Opt Express 2007;15(12):7522–7.
[28] Djerf T, Pallarès D, Johnsson F. Solids flow patterns in large-scale circulating fluidised bed boilers: Experimental evaluation under fluid-dynamically down-scaled conditions. Chem Eng Sci 2021;231:116309. https://doi.org/10.1016/j.ces.2020.116309.